NANO LETTERS

LETTER

pubs.acs.org/NanoLett

In Situ Characterization of Alloy Catalysts for Low-Temperature Graphene Growth

Robert S. Weatherup,[†] Bernhard C. Bayer,[†] Raoul Blume,[‡] Caterina Ducati,[§] Carsten Baehtz,[∥] Robert Schlögl,[⊥] and Stephan Hofmann*[,†]

[†]Department of Engineering, University of Cambridge, Cambridge CB3 0FA, U.K.

[‡]Helmholtz-Zentrum Berlin für Materialien und Energie, D-12489 Berlin, Germany

[§]Department of Materials Science and Metallurgy, University of Cambridge, Cambridge CB2 3QZ, U.K.

[∥]Institute of Ion Beam Physics and Materials Research, Helmholtz-Zentrum Dresden-Rossendorf, 01314 Dresden, Germany

[⊥]Fritz Haber Institute, D-14195 Berlin-Dahlem, Germany

Supporting Information

ABSTRACT: Low-temperature (~450 °C), scalable chemical vapor deposition of predominantly monolayer (74%) graphene films with an average D/G peak ratio of 0.24 and domain sizes in excess of 220 μm^2 is demonstrated via the design of alloy catalysts. The admixture of Au to polycrystalline Ni allows a controlled decrease in graphene nucleation density, highlighting the role of step edges. In situ, time-, and depth-resolved X-ray photoelectron spectroscopy and X-ray diffraction reveal the role of subsurface C species and allow a coherent model for graphene formation to be devised.

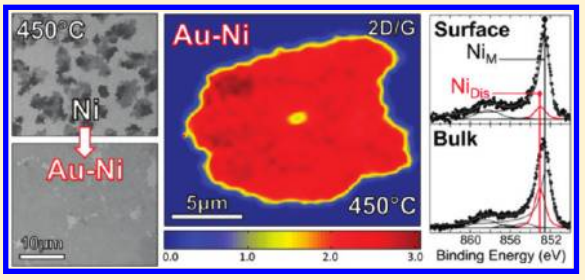

KEYWORDS: Graphene, chemical vapor deposition (CVD), alloy catalyst, in situ metrology, XPS, XRD

Scalable, economical growth is a key requirement to utilize the unique properties of mono- and few-layer graphene (M-/FLG) for electronic device applications. One of the most promising and versatile growth techniques for M-/FLG is catalytic chemical vapor deposition (CVD) in which transition metal surfaces are exposed to a gaseous carbon precursor at elevated temperatures. Graphene CVD over large areas has been demonstrated in particular with sacrificial polycrystalline metal films or foils of for instance Ni,[1−3] Ru,[4] or Cu.[5,6] However, with limited understanding of the detailed growth mechanism(s), growth control remains rudimentary. CVD optimization has in most cases focused empirically on the carbon dose and the process temperature profile.[7−9] Catalyst choice is typically guided by a low bulk C solubility and as-selected catalysts, for example, Cu, require excessive CVD temperatures of the order of 1000 °C, where considerable metal sublimation occurs. For lower-growth temperatures, the degree of graphitization and the average graphene domain size are reported to decrease. In particular for temperatures compatible with back-end CMOS integration (≤450 °C), carbon films with only nanocrystalline domains have been grown by thermal CVD[10,11] and highly defective FLG-based films are reported for plasma-assisted CVD.[12]

Unlike previous literature that focused on elementary metal catalysts, here we study catalyst alloying to create additional degrees of freedom for the optimization of M-/FLG CVD and rationalize the catalyst design by in situ metrology during growth. We show that alloying polycrystalline Ni with Au allows MLG CVD at temperatures of 450 °C with reasonable crystallinity and domain sizes larger than 15 μm. By combining high-pressure, time- and depth-resolved X-ray photoelectron spectroscopy (XPS) and in situ X-ray diffraction (XRD), we show that for Ni-based CVD, graphene growth occurs during isothermal hydrocarbon exposure and is not limited to a precipitation process upon cooling, as previously suggested.[1,2,13] Graphene nucleation is preceded by an increase in (subsurface) dissolved carbon with the formation of a solid solution of carbon in the catalyst material, which indicates that graphene CVD growth is not a purely surface process. We suggest that Au decorates a majority of high reactivity Ni surface sites, such as step edges, and lowers the stability of surface C.[14,15] The Au alloying thereby drastically lowers the graphene nucleation density, allowing more uniform and controlled growth. Designing bulk and surface alloy catalysts to tune reactivity and selectivity is an approach well-known in heterogeneous catalysis, but to our knowledge has not been demonstrated for graphene CVD, despite initial attempts to use catalyst alloying to control the bulk C concentration in precipitation experiments.[16]

We investigate sputter deposited, polycrystalline Ni films (~550 nm thick unless otherwise stated) on SiO_2(300 nm)/Si substrates covered with various thicknesses of thermally evaporated Au (0−10 nm). The samples are annealed and exposed to hydrocarbons in custom-built cold-wall reactors at low pressures [LPCVD, base pressures 5 × 10^{-7}mbar,

Received: June 17, 2011
Revised: August 11, 2011
Published: September 09, 2011

ACS Publications © 2011 American Chemical Society

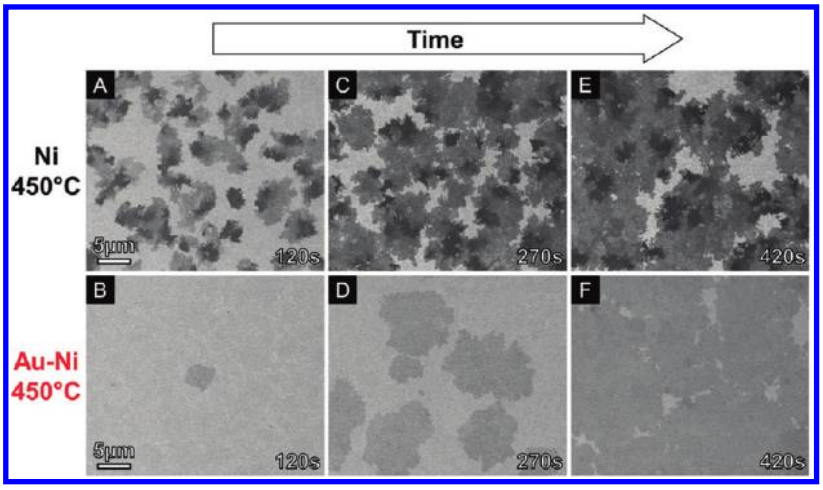

Figure 1. SEM micrographs of as-grown graphene [LPCVD, base pressure 5×10^{-7} mbar, 450 °C, C_2H_2(2×10^{-6}mbar), cooled at ~25 °C/min] for varying exposure times [120−420s] on Ni (A,C,E) and Au(5 nm)−Ni (B,D,F). Samples were preannealed at 600 °C in H_2(1mbar) for 15 min and then cooled to the growth temperature in H_2 (1mbar) at 25 °C/min. H_2 was then removed and the chamber pumped to $<1 \times 10^{-6}$ mbar, and the temperature stabilized over 3 min, prior to C_2H_2 exposure.

~450−600 °C, C_2H_2(2×10^{-6}mbar), cooled at ~25 °C/min] or in a hot-wall quartz tube furnace under atmospheric pressure [APCVD, ~900−1000 °C, CH_4(6−20 sccm)/H_2(600 sccm), cooled at ~25 °C/min]. The CVD results are compared to M-/FLG growth from a solid C precursor[17,18] for which we use films of tetrahedral amorphous carbon (ta-C) ~3 nm in thickness deposited using a filtered cathodic vacuum arc (FCVA) onto SiO_2(300 nm)/Si substrates. The ta-C was then covered with the same Ni and Au−Ni films as for the CVD process and annealed under vacuum to induce graphene growth [base pressures $\sim 5 \times 10^{-7}$mbar, ~600 °C, heated and cooled at ~25 °C/min].

In situ high-pressure XPS measurements during either LPCVD or vacuum heating were performed at the BESSY II synchrotron at the ISISS end station of the FHI-MPG. In situ (grazing incidence) XRD during LPCVD was performed at the European Synchrotron Radiation Facility (beamline BM20/ROBL, operated by the Helmholtz-Zentrum Dresden-Rossendorf). Samples were characterized ex situ, either as-grown or with the graphene films transferred to a SiO_2(300 nm)/Si substrate, using optical microscopy, scanning electron microscopy (SEM, FEI Philips XL30s, 1 kV), high-resolution transmission electron microscopy (HRTEM, JEOL JEM 4000EX, 400 kV), and Raman spectroscopy (Renishaw Raman InVia Microscope, 532 nm excitation). Transfer was carried out using polymethylmethacrylate (PMMA) to support the carbon films and a 0.5 M aqueous solution of $FeCl_3$ to remove the catalyst layer. For the Au−Ni catalysts, an additional etch in a solution of $KI/I_2/H_2O$ (4 g/1 g/40 mL) for 5 min was used to ensure removal of any remaining Au. We note that both the elemental Ni and the alloy Au−Ni catalyst films are efficiently etched away using this procedure.

Figure 1 compares SEM images of Ni and Au−Ni catalyst films after various C_2H_2 exposure times at 450 °C. For Au−Ni, graphene nucleii of homogeneous contrast grow and after ~420 s merge to an almost continuous graphene film. We refer to these regions that grow from a single nucleation point as domains, and we observe several of these domains in excess of 20 μm in lateral size without significant multilayer coverage (as seen by SEM contrast). Conversely, elemental Ni shows inhomogeneous, multilayer graphene domains for very short C_2H_2 exposures and at ~420 s regions of constant contrast are <3 μm, and complete coverage is not achieved. We emphasize that for all LP- and APCVD conditions considered, Au−Ni yields more uniform graphene films with fewer layers and much larger domain sizes.

Figure 2A shows typical Raman spectra for transferred M-/FLG films. A reduction in graphitic quality with reduced growth temperature is confirmed for the Ni catalyst between 600 and 450 °C by the significant increase in D/G peak ratio from 0.17 to 0.88 and G peak widening from 24 to 39 cm^{-1}. The addition of Au to the Ni catalyst at 450 °C leads to a 4-fold decrease in the D/G ratio from 0.88 to 0.20 with an accompanying reduction in G peak width from 39 to 14 cm^{-1}. In addition, increased monolayer coverage is obtained with the Raman spectra for 600 and 450 °C both showing 2D peaks that are well fitted by single Lorentzian curves and 2D/G peak intensity ratios >2 (2.36 and 2.10, respectively) confirming the presence of MLG.[19]

The optical image of a 35 × 35 μm region of a transferred graphene film grown on a Au(5 nm)−Ni catalyst at 450 °C (Figure 2B) shows contrast indicative of predominantly monolayer coverage with the few, small, lighter and darker regions indicative of areas of no graphene and FLG, respectively. Raman mapping of a region of this film confirms that 74% of the mapped area has a 2D/G peak intensity ratio of >2 and remaining regions all have a ratio >1.5 (Figure 2C). The D/G peak intensity map of the same area (Figure 2D) is reasonably uniform across the region with an average ratio of 0.24. Figures 2E,F show Raman maps of an individual domain grown under the same conditions as the continuous film but with a shorter exposure time (corresponding to Figure 1D). The 2D/G peak intensity ratio (Figure 2E) is >2 for almost the entire nucleus area (>220 μm^2), with only a small region (~1 μm^2) at the center with a ratio of ~1.5. The D/G peak intensity ratio (Figure 2F) is uniformly low throughout the central area of the nucleus with higher ratios (>1) around the edges, associated with edge defects.

We therefore confirm that the Au−Ni catalyst can yield continuous graphene films with predominantly monolayer coverage (74%) and domains with lateral dimensions in excess of 15 μm at 450 °C, which closely correlates with the domain sizes expected from SEM micrographs (Figure 1). We find that the majority of domains are MLG, and only a small proportion show

dx.doi.org/10.1021/nl202036y |*Nano Lett.* 2011, 11, 4154–4160

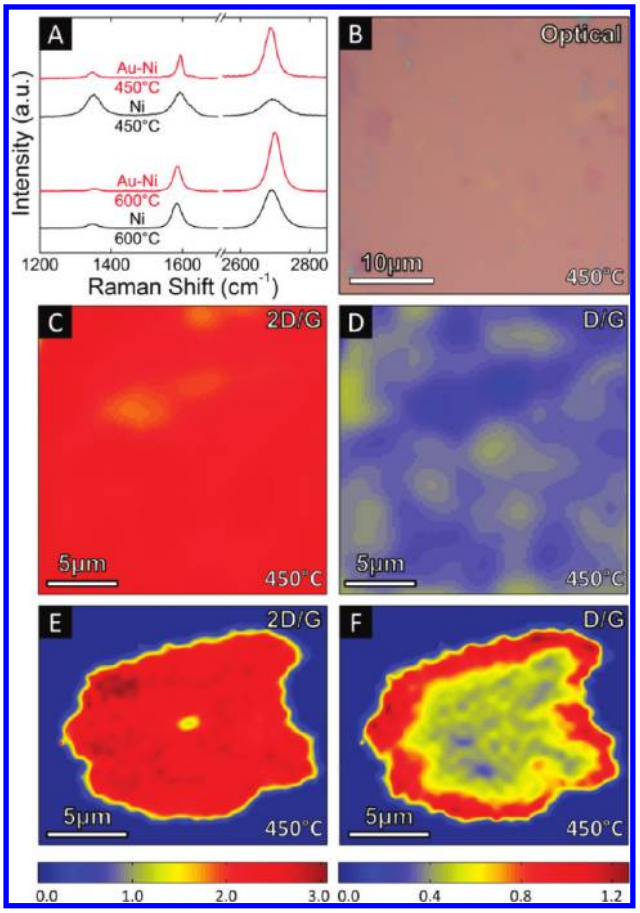

Figure 2. (A) Raman spectra of graphene films transferred to SiO_2(300 nm)/Si grown on Ni (black line) and Au(5 nm)−Ni (red line) by LPCVD at 600 and 450 °C. Optical image (B) and Raman maps of 2D/G peak intensity (C) and D/G peak intensity (D) of a continuous graphene film transferred to SiO_2(300 nm)/Si grown on Au(5 nm)−Ni by LPCVD (conditions as Figure 1.) with a 330 s exposure time. Raman maps of 2D/G peak intensity (E) and D/G peak intensity (F) for a graphene domain transferred to SiO_2(300 nm)/Si grown using the same catalyst and conditions as Figure 1D.

FLG regions, generally confined to the domain center. Figure 2E, F was chosen to highlight this aspect of the growth, which has similarities to reports of APCVD growth on Cu.[20] We also note that mapped areas corresponding to FLG commonly show a slight reduction in D/G peak intensity ratio (Figure 2C,D). We observe this trend throughout our Raman measurements confirming similar observations by Kondo et al.[21]

In order to develop an understanding of the underlying growth mechanism(s) and the origins of the notable improvements using Au−Ni catalysts, we use further ex situ measurements and detailed in situ probing.

It should first be noted that catalyst structure and composition are defined by annealing prior to the hydrocarbon exposure, which promotes grain growth and (for the bilayer films) the formation of Ni-rich solid solutions. On the basis of the Au−Ni bulk phase diagram,[22] we expect Ni-rich solid solutions at all of the given growth conditions, that is, the initial Au top-layer dissolves into the Ni film upon annealing. Assuming a homogeneous dissolution, initial 3, 5, and 10 nm Au top-layers correspond to approximately 0.4, 0.6, and 1.2 atom % bulk Au compositions, respectively.

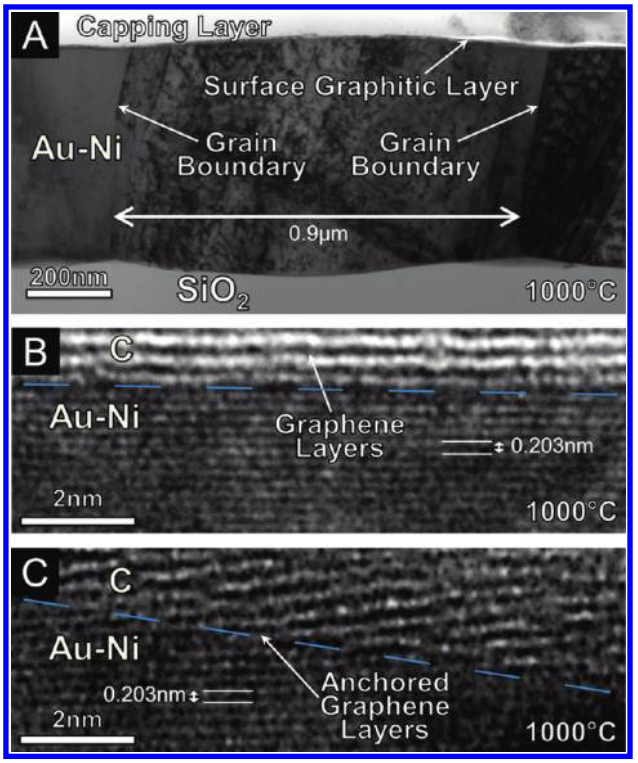

Figure 3. Au(10 nm)−Ni film after APCVD [~1000 °C, CH_4(10 sccm)/H_2(600 sccm), 3 min, cooled at ~25 °C/min]. Bright-field TEM image of a cross-section of the specimen (A). High-resolution TEM images of FLG−catalyst interface (emphasized by dashed blue lines), showing graphitic layers running parallel to the metal surface (B), and the anchoring of graphitic layers to the step edges of the Au−Ni film (C). The lattice spacings in the metal correspond to Ni(111).

Figure 3A shows a postgrowth cross-sectional TEM image of a Au(10 nm)−Ni catalyst film after APCVD at 1000 °C. Grain boundaries are seen to extend through the full thickness of the catalyst film and the average grain width of ~0.9 μm seen in cross-section is in agreement with plan-view SEM analysis of catalyst films annealed at 1000 °C. We note that the grain sizes for Ni and Au−Ni films are similar, excluding alloy induced changes in catalyst grain size from causing the observed differences in graphene growth. High-angle annular dark field (HAADF) profiles (not shown) of the Au−Ni layer shown in Figure 3 exhibit uniform contrast across the entire cross-section, that is, show no evidence for any significant localized Au enrichment after carbon exposure and cooling. The presence of Au within all regions of the catalyst film was confirmed by energy dispersive X-ray spectroscopy (EDX). No evidence of any structural Ni carbide phases is found by TEM (in agreement with XRD, see below). In situ XPS measurements of the $Au4f_{7/2}$ core level for Au(3 nm)−Ni samples confirm the presence of gold at the catalyst surface throughout the growth process (see Supporting Information Figure S1). The as-deposited catalyst shows a $Au4f_{7/2}$ spectra with similar peak positions to bulk Au but on heating to 600 °C, a small shift of ~0.2 eV in the $Au4f_{7/2}$ spectra, toward lower binding energies, is observed (see Supporting Information Figure S1). This can be attributed to surface alloy formation[23] for which Ni step edges provide preferential sites.[24] This shift remains on cooling to 450 °C, confirming Au−Ni alloying at the catalyst surface for the preannealed bilayer catalysts at the point of hydrocarbon exposure.

dx.doi.org/10.1021/nl202036y |Nano Lett. 2011, 11, 4154–4160

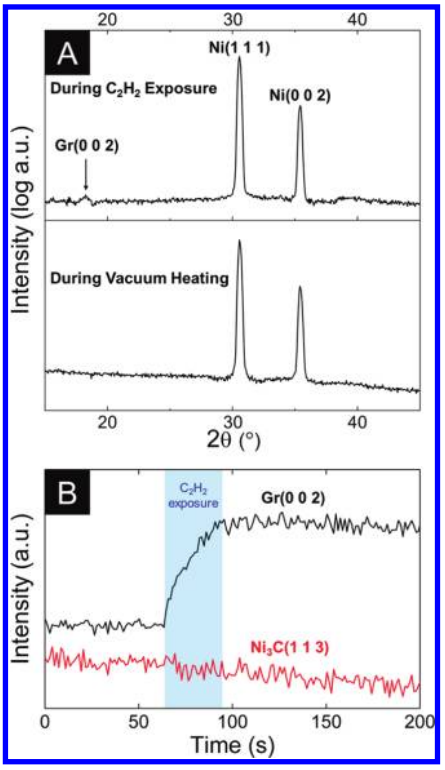

Figure 4. (A) In situ XRD diffractograms of Ni(~170 nm)/SiO_2-(200 nm)/Si at various stages of LPCVD. (B) Time-resolved plot of graphite (002) and $Ni_3C(113)$ peak intensities for Ni(~170 nm)/SiO_2(200 nm)/Si during LPCVD. A monochromatic X-ray beam of 11.5 keV, and a wavelength of 1.07812 Å (selected by a Si(111) double crystal monochromator) with an incident angle of $\alpha_i = 0.5°$ was used. Diffracted X-rays were measured using a horizontally aligned Soller slit system and a scintillation detector.

We find that 3−5 nm Au gives the best graphene uniformity with regards to our LP- and APCVD reference conditions with thicker Au layers leading to more inhomogeneous graphene layers that may be caused by incomplete alloying and Au island formation on the catalyst surface.[25] Attempts to grow on Au−Ni bilayers at 450 °C without preannealing yielded no graphitic growth, highlighting the importance of the alloy mixing. We note that mixing can alternatively be promoted by metal codeposition.

In Figures 3B,C, a high-resolution TEM image of the cross sectional specimen shows the interface between the Au-(10 nm)−Ni catalyst and several graphitic layers. The lattice spacings in the catalyst correspond to 0.203 nm, which matches the separation of Ni(111) planes. The effect of Au on the lattice parameters cannot be quantified from these HRTEM images. Graphene layers run parallel to the metal surface across the vast majority of the cross sectional sample (Figure 3B). Figure 3C shows a grain for which the interface is not parallel to the substrate normal (horizontal in this image), and thus has a higher density of step edges associated with it. Close to the interface, the (002) graphitic planes form an angle of ~7.5° to the Ni(111) planes, but progressively bend to align perpendicularly to the substrate normal. The graphitic layers appear anchored to the catalyst surface, demonstrating an important parallel to carbon nanotube growth.[26] This also relates to how additional graphene layers are formed in the case of the FLG centers seen for some domains on Au−Ni (Figure 2E).

In order to gain insight into the detailed catalyst behavior, we use in situ, time-, and depth-resolved XPS to monitor LPCVD based recipes. To complement the surface sensitive XPS, we use in situ, grazing incidence XRD with an estimated information depth of ~50 nm.

Figure 4A shows X-ray diffractograms at salient stages of the growth process. During heating of the catalyst film in vacuum we find sharp Ni(111) and Ni(200) reflections,[26,27] indicating that the Ni is metallic and of face-centered cubic (fcc) structure. Upon C_2H_2 exposure a weak graphite (002)[28] reflection develops, demonstrating that isothermal growth of FLG occurs upon the introduction of C_2H_2. The structure of the Ni remains virtually unchanged during exposure, and most notably, no bulk crystalline Ni-carbide[29,30] is formed. Further confirmation of this is obtained from Figure 4B, which shows the intensity of the graphite (002) and $Ni_3C(113)$ reflection positions as a function of time during C_2H_2 exposure. On the introduction of C_2H_2, the graphite signal rises almost immediately above the background and then continues to increase with further exposure, but immediately levels off when the C_2H_2 supply is removed. During the same C_2H_2 exposure, however, no (even temporary) rise in the carbide signal above background is observed, excluding even transient formation of crystalline Ni_3C. Longer (>60 min) exposures (not shown) confirm that the FLG growth is not self-limited but produces graphite-layers from metallic Ni with a constantly growing graphite (002) signal.

In situ XRD further allows a monitoring of the Ni lattice parameters during the CVD process. On the basis of Rietveld refinement of the Ni reflection positions in the 2θ range 27−67°, calibrated for thermal expansion, we find that during isothermal growth in C_2H_2(~1×10^{-4}mbar) an irreversible lattice expansion occurs, which is retained on C_2H_2 removal. At an exposure temperature of ~550 °C this lattice expansion is found to be 0.0010 ± 0.00016 Å. To confirm that carbon and not hydrogen (from C_2H_2) causes this expansion of the Ni lattice, we cross-checked that the lattice expansion due to H_2(~1 mbar) exposure for our CVD temperatures (450−750 °C) is reversed on H_2 removal. Furthermore at the LPCVD pressures even this reversible effect from H_2 is found to be negligible. This clearly shows that a Ni−C solid solution in the bulk of the metal catalyst film is formed during graphene growth. The lattice expansion corresponds to 0.14 ± 0.02 atom % C, which is in good agreement with the phase diagram value of ~0.15 atom % at 550 °C.[31]

Figures 5 A,B compare the time-resolved evolution of XP C 1s core level spectra during C_2H_2 exposure at ~600 °C for a Ni and Au−Ni catalyst film. We focus on the appearance of four components at approximately 283.2 eV (C_A), 283.8 eV (C_{Dis}), 284.4 eV (C_{Gr}), and 284.8 eV (C_B) in the C 1s spectra reflecting the presence of distinct C species which evolve differently as growth proceeds on each catalyst. Figure 5C,D shows SEM micrographs of samples grown under similar conditions to the in situ XPS measurements. These are representative of an intermediate stage of growth, and again show that the presence of Au in the catalyst reduces the spatial variation in graphene thickness, with areas of constant contrast increasing from <10 μm^2 for Ni to up to 800 μm^2 for Au−Ni, which is correlated with the XPS results below.

On introduction of C_2H_2 at the growth temperature, C_A appears first for both catalysts (Figure 5A,B), but is significantly weaker for the Au−Ni catalyst. C_{Dis} appears next and grows in intensity with time, until C_{Gr} and C_B emerge concurrently. The ratio of these latter components varies noticeably for the two

dx.doi.org/10.1021/nl202036y |*Nano Lett.* 2011, 11, 4154–4160

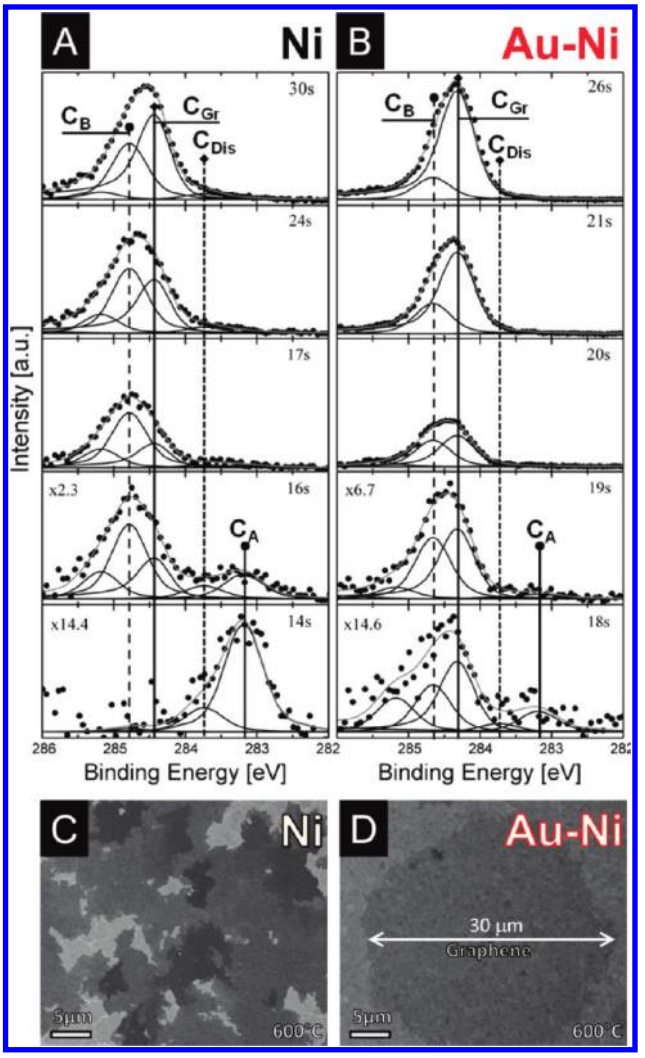

Figure 5. Time-resolved in situ XPS C1s core level lines for Ni (A) and Au(3 nm)−Ni (B) films during LPCVD. All spectra are collected in normal emission geometry at photon energies of 435 eV (surface sensitive; $\lambda_{escape} \approx 7$ Å) with a spectral resolution of ∼0.3 eV. The spectra are fitted using Doniach-Šùnjić functions convoluted with Gaussian profiles with an accuracy of ∼0.05 eV. Time signatures are relative to when the C_2H_2 valve is opened and spectral acquisition begins, however exposure pressure is not instantaneously reached. SEM micrographs of as-grown graphene [LPCVD, base pressure 5×10^{-7}mbar, 600 °C, C_2H_2(2×10^{-6} mbar), cooled at ∼25 °C/min] on Ni (C) and Au(3 nm)−Ni (D) representative of an intermediate stage of growth (2 min).

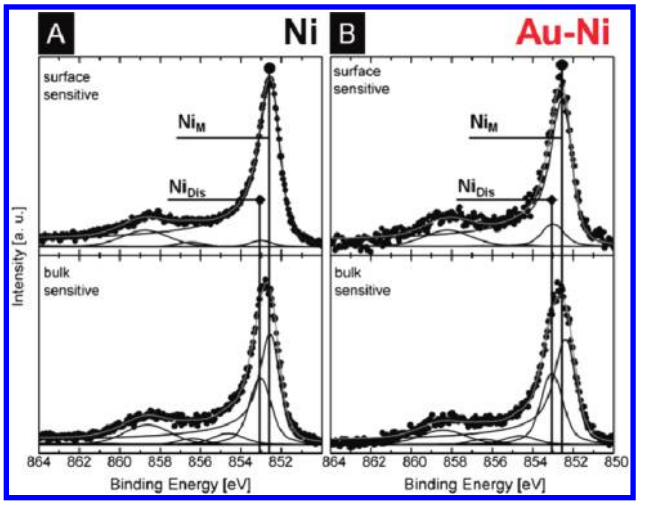

Figure 6. Depth resolved in situ XPS Ni2$p_{3/2}$ core level lines for Ni (A) and Au(3 nm)−Ni (B) films after LPCVD, before cooling. All spectra are background corrected (Shirley) and collected in normal emission geometry at photon energies of 1010 eV (surface sensitive; $\lambda_{escape} \approx 7$ Å) and 1300 eV (bulk sensitive; $\lambda_{escape} \approx 10$ Å) with a spectral resolution of ∼0.3−0.4 eV. Increased information depth is achieved using higher incident X-ray energies and hence increased electron mean free path lengths. The spectra are fitted using Doniach-Šùnjić functions convoluted with Gaussian profiles with an accuracy of ∼0.05 eV.

catalyst systems and with exposure time. C_B initially dominates for the Ni catalyst, and C_{Gr} for Au−Ni. C_{Gr} becomes increasingly prominent as growth proceeds and eventually becomes the dominant species for both catalyst systems, although the C_B component continues to be consistently higher for elemental Ni compared to Au−Ni.

C_A is a separate species appearing at the catalyst surface at start of growth (Figure 5A,B), and so we expect it to be related to surface C atoms at certain positions on the Ni. Recent results from graphene growth on Ir(111) catalyst films, which found a XP spectral component at a similar binding energy position,[32] indicate that these lattice positions may well be locations at step-edges or similar Ni defect sites. The formation of a Au−Ni surface alloy, and resulting decoration of a majority of high reactivity Ni surface sites such as step edges with Au,[24] is known to lower the stability of surface C[15]. The heavy suppression of C_A (Figure 5B) thus supports our assertion that C_A is related to surface C atoms at Ni defect sites.

In situ XPS measurements during the annealing/cooling of Ni/ta-C and Au(3 nm)−Ni/ta-C layer structures at ∼600 °C (not shown), show the presence of the same four peaks and a similar evolution of XPS core level signatures as for the LPCVD experiments. This indicates similar growth mechanisms for solid and gaseous carbon sources, and importantly that C_A cannot be assigned to simply an adsorbed gas species.[33] This is further corroborated by C_2H_2 exposures at 100 °C, which reveal adsorption/decomposition species at energies distinct from C_A in the C 1s spectra (283.46 eV for Ni, 283.48 eV for Au(3 nm)−Ni).

The interpretation of C_{Dis} is clarified by depth-resolved in situ Ni2$p_{3/2}$ core level spectra taken after growth at the exposure temperature (Figure 6). A peak is observed at 852.6 eV corresponding to metallic Ni (Ni_M) alongside a distinct component at 853.0 eV (Ni_{Dis}). The intensities of Ni_{Dis} and C_{Dis} correlate throughout our experiments, implying that these two components are related. Figure 6 shows that for both Ni and Au−Ni catalysts, Ni_{Dis} is more intense for "bulk" sensitive XPS conditions, indicating that Ni_{Dis}/C_{Dis} does not solely reflect a surface species and that our data is not consistent with a growth mechanism based on the transformation of a surface carbide such as Ni_2C.[34,35] We have already confirmed the presence of a Ni−C solid solution in the catalyst with no accompanying bulk carbide (Figure 4). Therefore, we assign Ni_{Dis}/C_{Dis} XPS signatures as dissolved C, rather than as a carbide phase, which is a common assignment in previous literature.[36−38]

We assign C_{Gr} as graphitic (sp^2 hybridized) carbon and C_B as deleterious (sp^3 hybridized) carbon or carbon at the periphery of graphene/FLG domains, based on comparison with other literature[32,33] and our previous XPS measurements on carbon

dx.doi.org/10.1021/nl202036y |Nano Lett. 2011, 11, 4154–4160

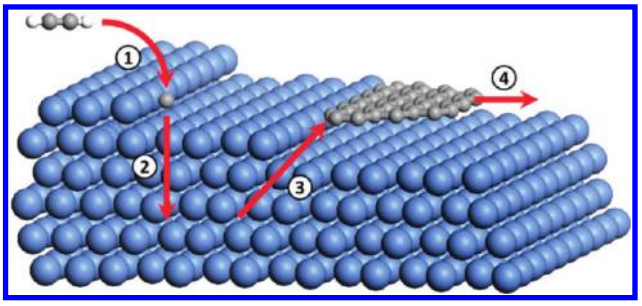

Figure 7. Schematic of proposed growth mechanism for graphene on Ni. (1) Hydrocarbon precursor dissociates on the catalyst surface. (2) C diffuses into the Ni subsurface/bulk. (3) Isothermal graphene nucleation occurs, preferentially at high reactivity Ni surface sites. (4) Individual domains expand under isothermal conditions until they coalesce.

nanotube CVD.[26,39] Hence, the suppression of C_B for Au−Ni catalysts compared to Ni indicates a reduction in defective, amorphous carbon as well as a decrease in the domain boundary density associated with larger graphene domain sizes, consistent with Figures 1 and 2. This reduction in C_B is preceded by a suppressed C_A component (Figure 5B), and this can be explained by a reduction in nucleation density due to fewer surface C atoms. The decreasing C_B/C_{Gr} peak ratio observed for both catalysts as growth proceeds is attributed to the decreasing proportion of edge atoms as domains grow. Our in situ measurements have therefore shown that C accumulates below the catalyst surface before M-/FLG growth occurs and that the Au admixture can suppress C anchoring at step edges/Ni defects.

On the basis of our in situ data we suggest a growth model, summarized in Figure 7. The hydrocarbon precursor dissociates on the catalyst surface (Step 1). The as-produced C binds to Ni surface sites (C_A) and diffuses into the Ni catalysts causing a lattice expansion throughout the catalyst bulk and a filling up of the subsurface region (C_{Dis}) (Step 2). Upon adequate C saturation, isothermal graphene nucleation occurs, preferentially at high reactivity Ni surface sites (Step 3), such as step edges, which may be dynamically stabilised during the process. This can be partially suppressed by Au decoration. Individual graphene domains then expand, under isothermal conditions, until they coalesce (Step 4). In the case of growth from solid carbon sources, the hydrocarbon dissociation step is replaced by a carbon dissolution step, but subsequent growth including the appearance of C adatoms (C_A) at the catalyst surface is otherwise the same.

This model is corroborated by various unconnected observations in earlier literature (isothermal graphene formation,[33,40,41] importance of step edges for graphene nucleation,[14,15,26,42,43] subsurface carbon increase[44]) and is also found to be consistent with in situ measurements during carbon nanotube growth under similar conditions,[45] and hence may be generally applicable to the catalytic growth of carbon nanostructures.

In summary, we show that by using an Au−Ni alloy catalyst the nucleation density of graphene is decreased and a drastic increase in the quality of graphene films is obtained enabling monolayer graphene growth of reasonable quality even at low (~450 °C), CMOS compatible CVD temperatures. In situ measurements allow us to devise a model of isothermal M-/FLG growth on Ni-based catalysts. Depth-resolved in situ XPS highlights the role of subsurface dissolved carbon species, indicating that the growth mechanism is neither limited to bulk precipitation upon cooling nor to a pure catalytic surface process. In combination with in situ XRD, the level of C dissolution into the catalyst can be quantified and both surface- and bulk-carbide formation can be excluded. The admixture of Au to poly crystalline Ni films allows us to experimentally verify the crucial role of step edges in graphene nucleation and also introduces the concept of rational catalyst design into graphene CVD.

■ ASSOCIATED CONTENT

Supporting Information. In situ XPS $Au4f_{7/2}$ core level lines for a Au(3 nm)−Ni film at salient stages of the CVD process (Figure S1). This material is available free of charge via the Internet at http://pubs.acs.org.

■ AUTHOR INFORMATION

Corresponding Author
*E-mail: sh315@cam.ac.uk.

■ ACKNOWLEDGMENT

We acknowledge the Helmholtz-Zentrum-Berlin Electron storage ring BESSY II for provision of synchrotron radiation at the ISISS beamline and we thank the BESSY staff for continuous support of our experiments. We acknowledge the European Synchrotron Radiation Facility (ESRF) for provision of synchrotron radiation facilities and we thank the staff for assistance in using beamline BM20/ROBL. The research leading to these results has received funding from the European Community's Seventh Framework Programme (FP7/2007-2013) under Grant Agreement 226716. R.S.W. acknowledges funding from EPSRC (Doctoral training award). C.D. and S.H. acknowledge funding from the Royal Society and S.H. acknowledges funding from EPSRC (Grant EP/H047565/1). We acknowledge Yuzheng Guo for assistance with Figure 7.

■ REFERENCES

(1) Yu, Q.; Lian, J.; Siriponglert, S.; Li, H.; Chen, Y. P.; Pei, S. S. *Appl. Phys. Lett.* **2008**, *93*, 113103.
(2) Reina, A.; Thiele, S.; Jia, X.; Bhaviripudi, S.; Dresselhaus, M. S.; Schaefer, J. A.; Kong, J. *Nano Res.* **2009**, *2*, 509.
(3) Kim, K. S.; Zhao, Y.; Jang, H.; Lee, S. Y.; Kim, J. M.; Kim, K. S.; Ahn, J. H.; Kim, P.; Choi, J. Y.; Hong, B. H. *Nature* **2009**, *457*, 706.
(4) Sutter, E.; Albrecht, P.; Sutter, P. *Appl. Phys. Lett.* **2009**, *95*, 133109.
(5) Li, X.; Cai, W.; An, J.; Kim, S.; Nah, J.; Yang, D.; Piner, R.; Velamakanni, A.; Jung, I.; Tutuc, E.; Banerjee, S. K.; Colombo, L.; Ruoff, R. S. *Science* **2009**, *324*, 1312.
(6) Bae, S.; Kim, H.; Lee, Y.; Xu, X.; Park, J.-S.; Zheng, Y.; Balakrishnan, J.; Lei, T.; Ri Kim, H.; Song, Y. I.; Kim, Y.-J.; Kim, K. S.; Özyilmaz, B.; Ahn, J.-H.; Hong, B. H.; Iijima, S. *Nat. Nanotechnol.* **2010**, *5*, 574.
(7) Li, X.; Magnuson, C. W.; Venugopal, A.; An, J.; Suk, J. W.; Han, B.; Borysiak, M.; Cai, W.; Velamakanni, A.; Zhu, Y.; Fu, L.; Vogel, E. M.; Voelkl, E.; Colombo, L.; Ruoff, R. S. *Nano Lett.* **2010**, *10*, 4328.
(8) Bhaviripudi, S.; Jia, X. T.; Dresselhaus, M. S.; Kong, J. *Nano Lett.* **2010**, *10* (10), 4128–4133.
(9) Lee, S.; Lee, K.; Zhong, Z. H. *Nano Lett.* **2010**, *10*, 4702.
(10) Rümmeli, M. H.; Bachmatiuk, A.; Scott, A.; Borrnert, F.; Warner, J. H.; Hoffman, V.; Lin, J. H.; Cuniberti, G.; Buchner, B. *ACS Nano* **2010**, *4*, 4206.

(11) Scott, A.; Dianat, A.; Börrnert, F.; Bachmatiuk, A.; Zhang, S.; Warner, J. H.; Borowiak-Paleń, E.; Knupfer, M.; Büchner, B.; Cuniberti, G.; Rümmeli, M. H. *Appl. Phys. Lett.* **2011**, *98*, 073110.
(12) Kim, J.; Ishihara, M.; Koga, Y.; Tsugawa, K.; Hasegawa, M.; Iijima, S. *Appl. Phys. Lett.* **2011**, *98*, 091502.
(13) Reina, A.; Jia, X.; Ho, J.; Nezich, D.; Son, H.; Bulovic, V.; Dresselhaus, M. S.; Kong, J. *Nano Lett.* **2009**, *9*, 30.
(14) Saadi, S.; Abild-Pedersen, F.; Helveg, S.; Sehested, J.; Hinnemann, B.; Appel, C. C.; Nørskov, J. K. *J. Phys. Chem. C* **2010**, *114*, 11221.
(15) Besenbacher, F.; Chorkendorff, I.; Clausen, B. S.; Hammer, B.; Molenbroek, A. M.; Nørskov, J. K.; Stensgaard, I. *Science* **1998**, *279*, 1913.
(16) Liu, N.; Fu, L.; Dai, B.; Yan, K.; Liu, X.; Zhao, R.; Zhang, Y.; Liu, Z. *Nano Lett.* **2011**, *11*, 297.
(17) Zheng, M.; Takei, K.; Hsia, B.; Fang, H.; Zhang, X.; Ferralis, N.; Ko, H.; Chueh, Y.-L.; Zhang, Y.; Maboudian, R.; Javey, A. *Appl. Phys. Lett.* **2010**, *96*, 063110.
(18) Saenger, K. L.; Tsang, J. C.; Bol, A. A.; Chu, J. O.; Grill, A.; Lavoie, C. *Appl. Phys. Lett.* **2010**, *96*, 153105.
(19) Ferrari, A.; Meyer, J.; Scardaci, V.; Casiraghi, C.; Lazzeri, M.; Mauri, F.; Piscanec, S.; Jiang, D.; Novoselov, K.; Roth, S.; Geim, A. *Phys. Rev. Lett.* **2006**, *97*, 187401.
(20) Robertson, A. W.; Warner, J. H. *Nano Lett.* **2011**, *11*, 1182.
(21) Kondo, D.; Sato, S.; Yagi, K.; Harada, N.; Sato, M.; Nihei, M.; Yokoyama, N. *Appl. Phys. Express* **2010**, *3*, 025102.
(22) Wang, J.; Lu, X.-G.; Sundman, B.; Su, X. *Calphad* **2005**, *29*, 263.
(23) Zafeiratos, S.; Kennou, S. *Appl. Surf. Sci.* **2001**, *173*, 69.
(24) Bengaard, H. S.; Nørskov, J. K.; Sehested, J.; Clausen, B. S.; Nielsen, L. P.; Molenbroek, A. M.; Rostrup-Nielsen, J. R. *J. Catal.* **2002**, *209*, 365.
(25) Jacobsen, J.; Pleth Nielsen, L.; Besenbacher, F.; Stensgaard, I.; Lægsgaard, E.; Rasmussen, T.; Jacobsen, K. W.; Nørskov, J. K. *Phys. Rev. Lett.* **1995**, *75*, 489.
(26) Hofmann, S.; Sharma, R.; Ducati, C.; Du, G.; Mattevi, C.; Cepek, C.; Cantoro, M.; Pisana, S.; Parvez, A.; Cervantes-Sodi, F.; Ferrari, A. C.; Dunin-Borkowski, R.; Lizzit, S.; Petaccia, L.; Goldoni, A.; Robertson, J. *Nano Lett.* **2007**, *7*, 602.
(27) Powder Diffraction File 04-0850. *JCPDS-International Centre for Diffraction Data*; Newtown Square: PA.
(28) Powder Diffraction File 89-8487. *JCPDS-International Centre for Diffraction Data*; Newtown Square: PA.
(29) Powder Diffraction File 72-1467. *JCPDS-International Centre for Diffraction Data*; Newtown Square: PA.
(30) Portnoi, V. K.; Leonov, a. V.; Mudretsova, S. N.; Fedotov, S. a. *Phys. Met. Metallogr. (Transl. of Fiz. Met. Metalloved.)* **2010**, *109*, 153.
(31) Singleton, B. M.; Nash, P. *Bull. Alloy Phase Diagrams* **1989**, *10*, 1221.
(32) Lacovig, P.; Pozzo, M.; Alfè, D.; Vilmercati, P.; Baraldi, A.; Lizzit, S. *Phys. Rev. Lett.* **2009**, *103*, 166101.
(33) Grüneis, A.; Kummer, K.; Vyalikh, D. V. *New J. Phys.* **2009**, *11*, 073050.
(34) Lahiri, J.; Miller, T.; Adamska, L.; Oleynik, I. I.; Batzill, M. *Nano Lett.* **2011**, *11*, 518.
(35) Lahiri, J.; Miller, T. S.; Ross, A. J.; Adamska, L.; Oleynik, I. I.; Batzill, M. *New J. Phys.* **2011**, *13*, 025001.
(36) Czekaj, I.; Loviat, F.; Raimondi, F.; Wambach, J.; Biollaz, S.; Wokaun, A. *Appl. Catal., A* **2007**, *329*, 68.
(37) VijaiBharathy, P.; Chang, Y.-Y.; Nataraj, D.; Yang, Q.; Yang, S.-M.; Mangalaraj, D.; Yang, L.; Webster, T. J. *Thin Solid Films* **2010**, *519*, 1623.
(38) Zdansky, E. O. F.; Nilsson, A.; Martensson, N. *Surf. Sci.* **1994**, *310*, L583.
(39) Hofmann, S.; Blume, R.; Wirth, C. T.; Cantoro, M.; Sharma, R.; Ducati, C.; Hävecker, M.; Zafeiratos, S.; Schnoerch, P.; Oestereich, A. et al. *J. Phys. Chem. C* **2009**, *113*, 1648.
(40) Li, X.; Cai, W.; Colombo, L.; Ruoff, R. S. *Nano Lett.* **2009**, *9*, 4268.
(41) Shelton, J.; Patil, H.; Blakely, J. *Surf. Sci.* **1974**, *43*, 493.
(42) Gao, J.; Yip, J.; Zhao, J.; Yakobson, B. I.; Ding, F. *J. Am. Chem. Soc.* **2011**, *113*, 5009.
(43) Sutter, P. W.; Flege, J. I.; Sutter, E. A. *Nat. Mater.* **2008**, *7*, 406.
(44) Wiltner, A.; Linsmeier, C.; Jacob, T. *J. Chem. Phys.* **2008**, *129*, 084704.
(45) Rinaldi, A.; Tessonnier, J.-P.; Schuster, M. E.; Blume, R.; Girgsdies, F.; Zhang, Q.; Jacob, T.; Abd Hamid, S. B.; Su, D. S.; Schlögl, R. *Angew. Chem., Int. Ed.* **2011**, *50*, 3313.